

# **Friction and Wear Behaviour of Plasma Sprayed Fly Ash Added Red Mud Coatings**

**Abstract:** The present investigation aims at evaluating the effect of fly ash addition on sliding wear behaviour of pure red mud. Plasma sprayed coatings composed of red mud and varying percentage of fly ash were considered for the wear behavior study. Plasma spraying technique was involved at different levels of operating power (6, 9, 12 and 15 kW). Investigations of the coatings **focused** on the basis of some tribological properties like sliding wear behaviour, wear morphology, wear mechanism and frictional force. Experimental investigations also include the effect of varying percentage of fly ash on dry sliding wear behaviour of pure red mud. Fly ash with 10, 20 and 50 % by weight was mixed with red mud and allowed for the sliding wear test using pin on disc wear test machine. The wear test was performed for sliding distance **up to 942 m** with track diameter of 100 mm and at sliding speed of 100 rpm (0.523 m/s); applying normal load of 10 N for a maximum duration of 30 minutes. The plots pertaining to the variation of wear rate and frictional force with that of sliding distance and time has been presented. Significant wear resistance being visible with the addition of fly ash due to increase in bond strength and dense film at interface. **Wear rate decreases with operating power up 12 kW thereafter declines initiating other dominating parameters.**

**Key words:** Red mud; Fly ash; Plasma Coating; Sliding wear; Wear morphology; Frictional force; wear mechanism.

## **1. INTRODUCTION:**

Coating technologies have already gained **a** promising momentum for the creation of emerging materials in the last few decades. Coatings with some advanced wear properties put a signature of claiming for the better use in tribological applications. Plasma spray is one of the most widely used techniques involved in surface modification by augmentation of wear resistance, which may affirm the great versatility and its application to a wide spectrum of materials. The coatings with considerable amount of hardness can protect against variety of wear mediums including abrasive, adhesive and corrosive. **Basically, wear resistive coatings are fabricated by considering some common conventional materials like nickel, iron, cobalt**

33 and molybdenum based alloys [1-2]. Extensive investigations pertaining to the erosion wear  
34 behavior of plasma sprayed ceramic coatings by using Taguchi Technique being reported by  
35 some experimenters [3]. The tribological properties of traditional manganese phosphate  
36 coatings and hBN composite coatings composed of nano hexagonal boron nitride (hBN) in  
37 layered manganese phosphate crystals on AISI 1040 steel were being divulged in some  
38 literatures [4].

39 In retrospection, literatures made available regarding the wear behaviour of WC with 12% Co  
40 coatings produced by Air Plasma Spraying method at different standoff distances [5].  
41 Examinations on the basis of the wear behaviour of Mo and Mo+NiCrBSi thermally sprayed  
42 coatings being performed for the application as next generation ring face coatings [6]. Almost  
43 all plasma sprayed ceramic coatings portrayed favorable tribological performance in linear  
44 contact at high temperatures: high anti-wear resistance and easy to be lubricated owing to the  
45 oil storage of pores in coatings [7-9]. But needful to say, plasma sprayed ceramic coatings  
46 exhibit some failure mechanisms during sliding such as plastic deformation, brittle fracture  
47 and polish effects [10], which in turn demands a few additives, which could reduce the  
48 friction and wear of plasma sprayed ceramic coatings [11].

49 Several factors may influence the tribological behaviour of a coated surface ramified as: the  
50 geometry of the contact including macro geometry and topography of the surfaces; the  
51 material characteristics; basic mechanical properties as well the microstructure and finally the  
52 operating parameters controlling the coating deposition [12].

53 Red mud as an industrial waste material is considered to be the material of choice for coating  
54 applications. It is behooved to mention here that, red mud in present decade should be  
55 considered as an alternative wealth for replacing some conventional expensive coating  
56 materials. Utilization of red mud and its implications made available in literature [13] in great  
57 details. Few results on the basis of wear behavior of red mud were being reported by some  
58 researchers. In addition to above, morphology and solid particle erosion wear behaviour of red  
59 mud and fly ash composite were being available in literature [14]. Characteristics of plasma  
60 sprayed pure red mud coatings were being reported [15]. Red mud as filling material is also  
61 found to be the wear enhancing agent for metals [16]. Data pertaining to the sliding wear  
62 behavior of fly ash based red mud composite coatings are not abundant and need to be  
63 addressed. The present investigation is an attempt in a direction to evaluate the wear behavior  
64 of varying percentage of fly ash with pure red mud coating at different operating power  
65 subjected to normal laboratory conditions. This paper may pave the path for furthering the  
66 study to throw some further light on fly ash based red mud coatings.

67

## 68 2. MATERIALS AND METHODS OF EXPERIMENTATION

### 69 2.1 Preparation of coating powder

70 The present experimental work included the preparation of coating powder considering the  
71 raw materials as red mud and fly ash powders. The powder mixture concomitants of red mud  
72 and different percentage of fly ash was being prepared and mixed using V-shaped drum  
73 mixer. In addition, pure red mud powder was also considered as coating material for the sake  
74 of comparison on the basis of percentage of fly ash addition. Coating of the various  
75 combinations of mixed powders was conducted on one side cross section of the mild steel  
76 substrate. Data pertaining to Table 1 contains the different combinations of the mixtures  
77 chosen for plasma spraying.

78

**Table. 1** Powders used for coating deposition.

Sl.No.	Coating Material	Mixture Composition (By weight %)
1	Red Mud (RM)	100
2	Red Mud + Fly Ash (FA)	90 + 10
3	Red Mud + Fly Ash	80 + 20
4	Red Mud + Fly Ash	50 + 50

79 Red mud, as the primary raw material was collected in powder form from National  
80 Aluminium Company (NALCO) located at Damonjodi in the state of odisha, India. The as-  
81 received powder was sieved to obtain particles in the required size range of 80-100  $\mu\text{m}$ . Raw  
82 fly ash was collected from the captive power plant of Rourkela steel plant, India and allowed  
83 for sieving to maintain same size range as that of fly powder. Powders having three different  
84 weight ratios of red mud and fly ash (Table 1) were extensively prepared by mixing  
85 thoroughly.

### 86 2.2 Preparation of substrates

87 Commercially available mild steel rod was mooted as source for substrate preparation. The  
88 rod was cut to some number of pieces having one particular dimension ( $l = 40$  mm and  $\text{Ø} = 12$   
89 mm) each. The specimens were grit blasted from one side cross section (initial roughness 0.03  
90 mm) at a pressure of  $3 \text{ kg/cm}^2$  using alumina grits of grit size 60. The stand-off distance in the  
91 shot blasting was kept between 120-150 mm. Then the average roughness of the substrate was  
92 reported to be  $6.8 \mu\text{m}$ . The grit blasted specimens were allowed for plasma spraying after  
93 cleaning in an ultrasonic cleaning unit.

94

### 95 2.3 Plasma spraying

96 The spraying process was performed at the Laser and Plasma technology division of  
97 **Bhabha** Atomic Research Centre, Mumbai, India by adopting conventional atmospheric

98 plasma spraying (APS) set up. The plasma input power was varied from 6 to 15 kW by  
 99 controlling the gas flow rate, voltage and arc current. The powder feed rate was maintained to  
 100 be constant at 10 gm/min by using a turntable type volumetric powder feeder. Plasma  
 101 generation demanded the suitability by purging Argon as primary and Nitrogen as secondary  
 102 gas agent. The mixture of powders were deposited at spraying angle of 90° by maintaining the  
 103 powder feeding as external to the gun. The properties of the coating are merely depends upon  
 104 the parameters of spraying process. The operating parameters maintained during coating  
 105 deposition process are being tabulated in Table.2.

106

**Table 2** Operating parameters during coating deposition

Operating Parameters	Values
Plasma Arc Current (Ampere)	200,225,250,300
Arc Voltage (Volt)	30,40,48,50
Torch Input Power (kW)	6,9,12,15
Plasma Gas(Argon), (litre/min)	20
Secondary Gas(Nitrogen),(litre/min)	2
Career Gas(Argon) Flow rate (litre/min)	7
Powder Feed Rate (gm/min)	10
Torch to base distance (mm)	110
Arc Length Range (mm)	2,3,6,8,11

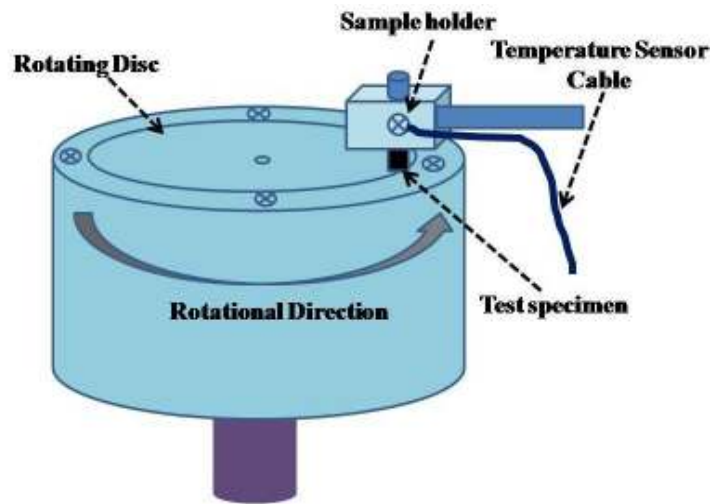
107 *2.4 Pin on disc Wear Testing*

108 The above experiment was being conducted in the pin on disc type friction and wear  
 109 monitor (DUCOM; TR-20-M100) with data acquisition system. The concerned machine was  
 110 used to evaluate the wear behavior of the coatings against hardened ground steel disc (En-32)  
 111 having hardness of 65 HRC and surface roughness (Ra) 0.5 µm. The versatility of the  
 112 equipment lies behind the design to study the wear behaviour under un-lubricated sliding  
 113 condition, which occurs between a stationary pin and a rotating disc.

114 The disc of the machine rotates with the help of a D.C. motor having speed range of 0-200  
 115 rpm with wear track diameter 0-160 mm; which can yield sliding speed of 0-10 m/s. Load is  
 116 to be applied on pin (specimen) by dead weight through pulley string arrangement. The  
 117 system has a maximum loading capacity of 500 N. For the present experimentation, pin  
 118 specimen was kept stationary perpendicular to disc, while the circular disc was rotated as  
 119 shown in Figure 1.

120

121



122  
123

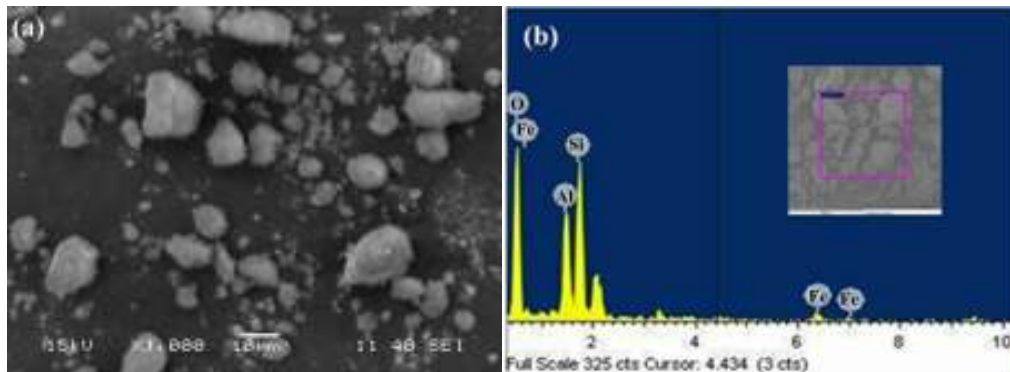
124 **Figure.1** Schematic Representation of Pin on Disc Apparatus

125 **3. RESULTS AND DISCUSSION**

126 *3.1 Scanning electron microscopy and Compositional analysis*

127 The characterization of red mud powder involved taking microstructures by the help of  
 128 Scanning electron microscope (JEOL; JSM-6480 LV). The micro structural images captured  
 129 by SEM (Scanning electron microscope) and EDS (energy dispersive spectroscopy) analysis  
 130 of pure red mud powder were being illustrated in Figure 2. EDS experiment was performed  
 131 by the **above SEM** with the required attached module. Data presented in Table 3 indicates the  
 132 weight as well the atomic percentage of elements comprising pure red mud powder. The EDS  
 133 analysis of red mud revealed the signature of some elements like Fe, Al, Si, O and some other  
 134 minor constituents. The prominent constituent of red mud was found to be iron with its  
 135 oxides. The EDS analysis of red mud with 20 % fly ash coatings prepared at 9 kW of  
 136 operating power **is** shown in Figure 3. In addition, the analogous elemental analysis relating  
 137 Figure-3 **is** reported in Table.4, indicating the increase in silica and iron constituents in the  
 138 composite coating.

139



140  
141

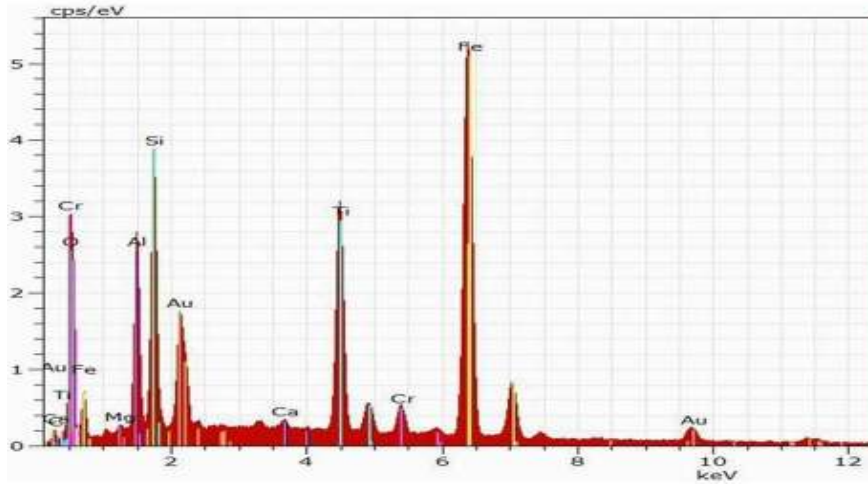
Figure 2. (a) SEM and (b) EDS analysis of Red Mud

142

143

**Table3.** Elemental analysis of Red mud

Element	Weight%	Atomic%
C K	24.59	33.29
O K	23.65	24.54
Al K	7.41	4.47
Si K	12.21	7.07
Fe K	32.14	30.62
Totals	100.00	



144

145

Figure 3. EDS analysis of RM+20 % FA Composite coating at 9 kW

146

147

**Table4.** Elemental analysis of RM+20 % FA Composite coated at 9 kW

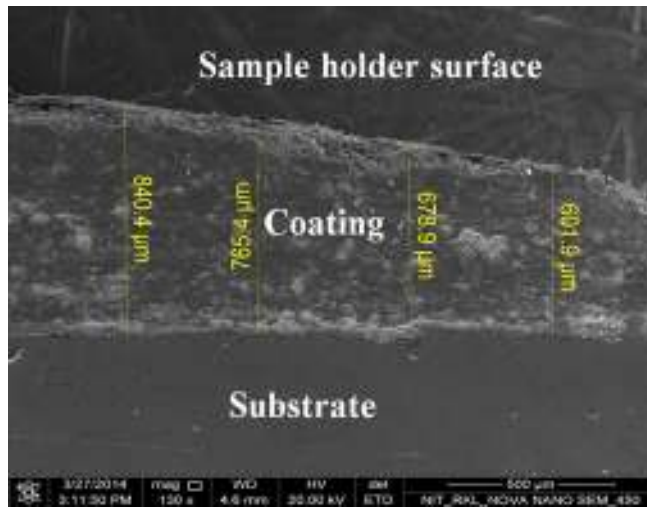
Element	Weight %	Atomic %
Fe K	36.13	25.90
O K	21.74	42.61
Ti K	14.02	9.18
Si K	17.10	7.93
Al K	6.59	7.66
Cr K	2.14	1.29
C K	1.99	5.20
Ca K	0.29	0.22
Au K	0.00	0.00
Mg K	0.00	0.00
Totals	100 %	100

148

149

150 3.2 Coating porosity

151 Image analysis technique was adopted for the measurement of porosity of coating  
 152 materials. The polished surfaces of various coatings were kept under a microscope (Neomate)  
 153 equipped with a charge coupled-device (CCD) camera (JVC, TK 870E). Volume of interest  
 154 (VOIS) image analysis software paid an important role for the determination of porosity. The  
 155 software can measure accurately the total area captured by the objective of the microscope.  
 156 Hence the total area and the area covered by the pores are separately measured to report  
 157 porosity. The “VOIS image analysis software” used in this analysis is being licensed by the  
 158 authors. The porosity data of three different coating powders are being tabulated in Table.5. A  
 159 cross sectional view of red mud coating prepared at 9 kW of operating power was captured by  
 160 the help of field emission scanning electron microscope (FESEM; Nova Nano SEM-450), as  
 161 shown in Figure 4.



162

163

**Figure 4.** FESEM image of coating Cross section of pure red mud at 9 kW

164

**Table 5.** Coating Porosity for different coating type.

Coating Material	Plasma Torch Input Power(kW)	Porosity (%)
Red Mud	6	12.89
	9	12.02
	12	11.87
	15	13.02
90 % Red Mud + 10 % Fly Ash	6	11.52
	9	11.12
	12	10.90
	15	12.98
80 % Red Mud + 20 % Fly Ash	6	10.89
	9	10.54
	12	10.17
	15	11.78

165 Approximately 8-13% porosity range was observed (Table-3) for all three coating  
 166 materials. Porosity amount was found to be ameliorated in case of all coating compositions  
 167 prepared at lower (6 kW) and at higher (15 kW) power levels. At 6 kW operating power level,  
 168 there is poor melting of particles subjected to relatively low plasma gas temperature  
 169 exhibiting non-uniform mixing of molten particles; which in turn causes reasonably porous  
 170 coating layer. On the other hand, at highest operating power level (15 kW) the high plasma  
 171 gas temperature caused faster deposition of molten particles by creating thickened coating  
 172 layer with less hardness and high porosity.

173 Porosity level was found to be higher in case of pure red mud compared to the composite  
 174 coatings pertaining to the mixture of fly ash and red mud. About 3-10% porosity level was  
 175 reported for the coatings prepared by conventional plasma spraying [17], which supports the  
 176 porosity results as obtained in the present investigation.

### 177 3.3 Coating Hardness

178 The polished section of the coatings put under optical microscope for the microscopic  
 179 observations, which revealed the presence of three distinguishable different phases namely  
 180 dull, white and spotted. The three different distinct phases are allowed for micro indenting to  
 181 record micro hardness data with the help of Leitz micro hardness Tester using 50 Pa (0.493 N)  
 182 on all samples. The results are summarized in Table.6. The three structurally different phases  
 183 of red mud coatings bear three different ranges of hardness values varying from 488 to 588  
 184 HV. Hardness values were found to be enhanced for the composite coatings belonging  
 185 mixture of red mud and fly ash. This result is attributed due to the increased content of  
 186 alumina and silica in the composition of feed material forming alumino-silicate (mullite  
 187 phase) during spray deposition [18].

188 **Table 6.** Coating Hardness for different operating power level

Coating Material	Plasma Torch Input Power (kW)	Micro Hardness (HV)		
		Dull	White	Spotted
100% Red Mud	6	540	488	496
	9	532	498	511
	12	586	513	508
	15	555	502	510
90% Red Mud + 10 % Fly Ash	6	638	632	628
	9	648	642	636
	12	660	638	628
	15	651	640	632
80 % Red Mud + 20 % Fly Ash	6	658	649	642
	9	669	658	649
	12	699	689	652
	15	681	681	650
50 % Red Mud + 50 % Fly Ash	6	696	679	658
	9	682	633	672
	12	726	712	660
	15	719	679	668

189 3.4 Wear test study

190 Prior to the starting of the wear testing experiment, the pin and the disc surface of the  
191 concerned equipment were polished perfectly with emery papers for better ensuring of smooth  
192 contact with the coating samples. Hereafter the surface roughness lessens by a magnitude of  
193 0.1  $\mu\text{m}$ . The wear tests were carried out as per ASTM G- 99 standard for maximum time  
194 period of 30 minutes under un-lubricated condition in a normal laboratory ambience having  
195 relative humidity of 40-55% and the temperature range of 20-25°C. The weight of the  
196 specimens before and after the wear experiment were being recorded by using electronic  
197 weighing machine having accuracy up to second decimal limit (0.01 mg) for monitoring the  
198 mass loss occurrence in the coating samples. Specimens were taken care of in particular for  
199 cleaning with woolen cloth to avoid entrapment of wear debris and to maintain uniformity in  
200 each set of experiments. The test pieces are cleaned with tetrachloroethylene solution before  
201 and after each test. Wear rate was estimated by measuring the mass loss ( $\Delta m$ ) in the specimen  
202 after each test. Wear rate relating to mass loss and the sliding distance (L) was formulated  
203 below in equation (1).  
204

$$W_r = \frac{\Delta m}{L} \quad (1)$$

205 Where  $W_r$  = Wear rate in N/m;

206  $\Delta m$  = Mass Loss in Newton (N);

207  $L$  = Sliding distance in meter (m).

208 The frictional force (F) was measured directly from the apparatus in 'kg' at each time  
209 interval.

210 The wear experiment was carried out at normal atmospheric temperature under a constant  
211 normal force of 10 N and a fixed speed of 100 rpm. The track diameter of the equipment was  
212 kept at 100 mm. The maximum duration of sliding was 30 minutes comprising of 10 intervals  
213 with each having 3 minutes of time gap. Each sample specimen was allowed for sliding for  
214 distinct time interval.

215 Initially, the experiment was performed with red mud coated samples and then continued  
216 for fly ash based red mud coating composites. Figure 5 illustrates the variation of wear rates  
217 with sliding distance for different operating power levels.

218 The wear results for pure red mud coating operated at 6 kW of operating power being  
219 visible in Figure 5 (a) disclosing the variation of wear rate with minimum value of 0.11 N/m  
220 to maximum value of 0.45 N/m. The wear rate value was found to be increased from 0.11 to  
221 0.13 N/m for first 6 minutes of sliding. The wear rate plot affirmed a plateau just after a  
222 drastic increasing trend from 6 to 12 minutes of duration. The plateau in wear rate value may  
223 be attributed due to the variation of coating layer property. This is one fact indicating the  
224 more hardness of denser surface of top layer than that of bulk layer. The change of coating  
225 property just after 6 minutes of sliding may be due to the coating property variations bearing  
226 less hardness of bulk layer.

227 The wear rate was reduced for fly ash based (10%, 20% and 50%) composite coatings, as  
228 being illustrated in Figure 5. This indicative trend of wear rate for fly ash composite coatings  
229 are quite similar to that of pure red mud coating. Substantial slow increase in wear rate for the  
230 composite coatings was being visible followed by a drastic gain. Henceforth, the wear rate  
231 was constant for all composite coating type. The plots pertaining to Figure 6 represent the  
232 variation of wear rates of each coating type with that of sliding distance for different operating  
233 power level.

234 The effect of operating power level on wear rate is quite interesting. The wear rate is  
235 resulted attributing to the porosity and hardness. The wear rate was found to be enhanced up  
236 to 12 kW and departing result for 15 kW. The wear rate for 15 kW was found to be lied  
237 between 9 and 12 kW. This might be due to the improper particle to particle bonding and poor  
238 stacking to the substrate, which in turn lowered the hardness as well as density due to poor  
239 interfacial bond strength. Figure 7 shows the trends of wear rate for all coating materials  
240 against operating power level for a particular sliding time (15 minutes).

241 An experimental study on coating thickness for fly ash and red mud composite with  
242 operating power is reported [18]. An increase in coating thickness with increase in input  
243 power to the plasma torch; up to about 12 kW is observed and then with further higher input  
244 power no improvement in coating thickness is recorded.

245 The frictional force (F) in kg was measured directly from wear apparatus deputed for the  
246 present investigation. The graphical representation concerning the variation of frictional  
247 forces with that of sliding time is focused on Figure 8, which includes the picture for all  
248 coating materials and also for operating power levels considered. As per the observations,  
249 maximum frictional force is evidenced for pure red mud coating and being decreased with the  
250 addition of fly ash, akin to the results as being occurred for wear rate. An increase in frictional  
251 force up to a maximum value of 0.63 kg for pure red mud coating at 12 minute sliding time is  
252 observed followed by a fluctuating wavy response up to 21 minutes then a constant magnitude  
253 up to 30 minute of sliding.

254

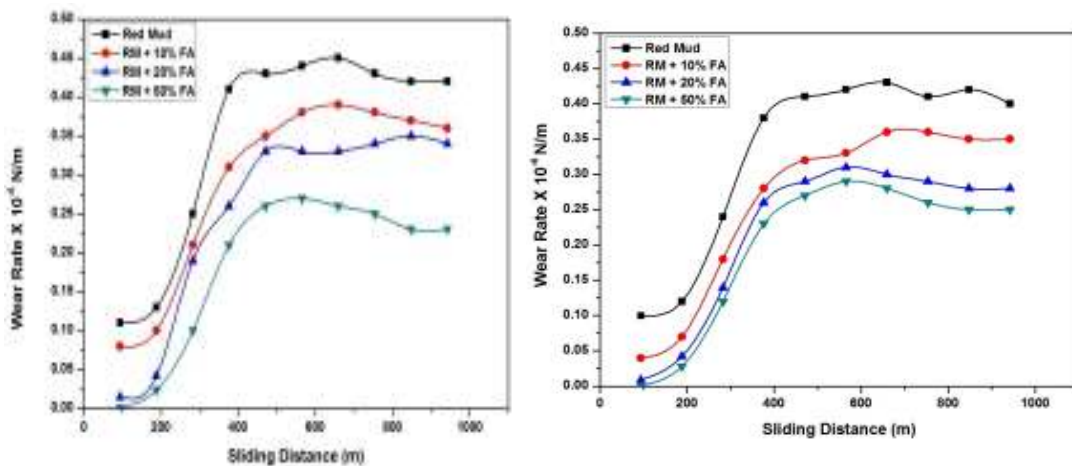
255 Figure 9 shows the comparative study relating frictional forces for the coating composites  
256 with 10% fly ash. The frictional force is found to be maximum at 6 kW and be minimum at 12  
257 kW operating power. At 15 kW of operating power, the frictional force was reported to be in  
258 range of values whatever lies for the power levels in between 9 to 12 kW. These results are in  
259 accordance with the findings as being observed for wear rates.

260

261 Wear morphology for selected coating samples were being highlighted in some images  
262 captured by FESEM. Figure 10 represents the wear morphological images for red mud with  
263 10% fly ash coating (prepared at 6 kW operating power) allowed for sliding for the time  
264 intervals of 3, 6, 12 and 15 minutes. Owing to continuous sliding of counter surfaces, wear  
265 debris formed which interlocks within sliding interface attributing pitting and eventually crack  
266 formation. Wear scars, debris formed and cracked sections are being clearly visible in Figure  
267 10 (b) and Fig 10 (d) assigning to a fatigue failure in the real sense on the worn surface.  
268 Figure 11 shows the worn surfaces for 50 % fly ash based red mud coatings (prepared at 12

269 kW of operating power level) for the sliding intervals 3, 6, 12, 15, 27 and 30 minutes. The  
 270 wear morphology changes with increase in the sliding distance impacting change in surface  
 271 roughness leading to the interruption of its contact mechanism. The change in wear  
 272 characteristics may be attributed due to the variation of hardness of coating inter-layers with  
 273 respect to the change in sliding distance. At incipient, a slow increase in wear rate is observed  
 274 and then attains a rapid increment, the 'break in' situation, after traversing of certain sliding  
 275 distance. The further increase in sliding distance cannot change the contact area; causing a  
 276 relatively steady wear rate. Hence, it can be concluded that the wear takes place by the  
 277 phenomenon of adhesion and abrasive mechanism due to development of shear stresses in  
 278 between the hard asperities of the two surfaces in contact. After the "break in" phase, the  
 279 trend of wear rate remains almost constant for coatings deposited at all power levels. The  
 280 duration of this stage extends till the end of the test.

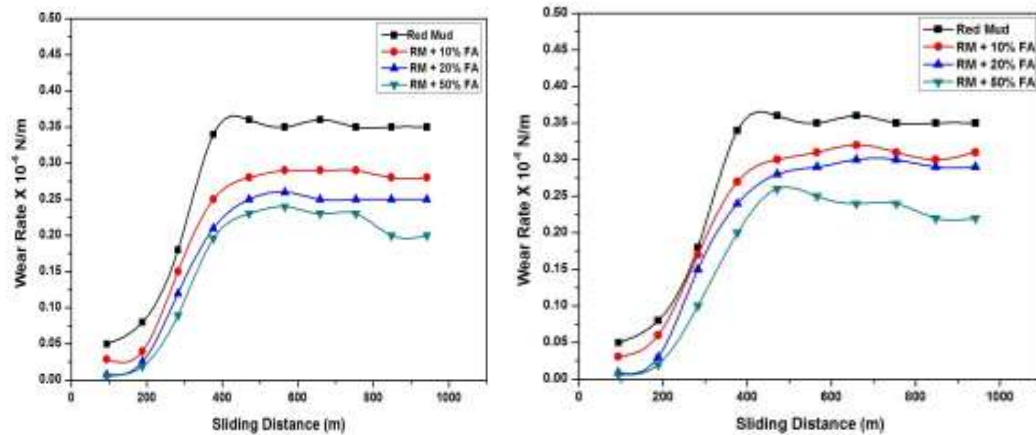
281



282

(a)

(b)



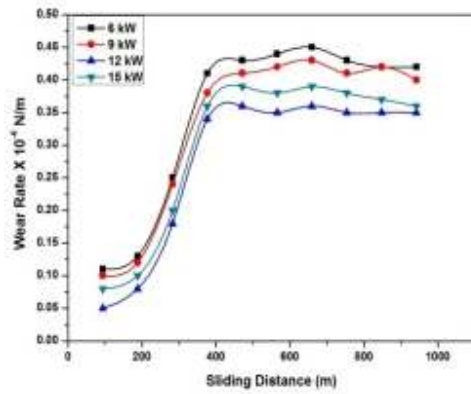
283

(c)

(d)

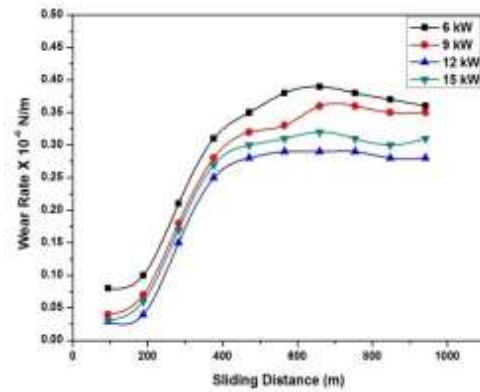
284

285 Figure.5. Wear Rates obtained for different coating type with sliding distance. (a) 6 kW, (b) 9  
 286 kW, (c) 12 kW, (d) 15 kW.

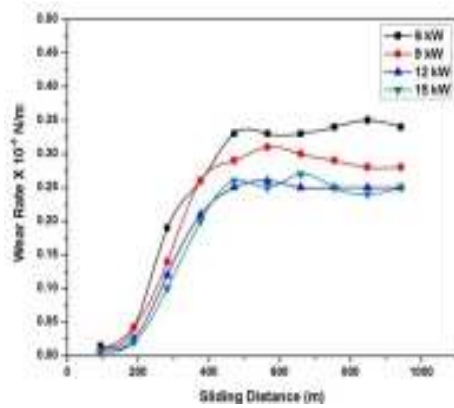


287

(a)

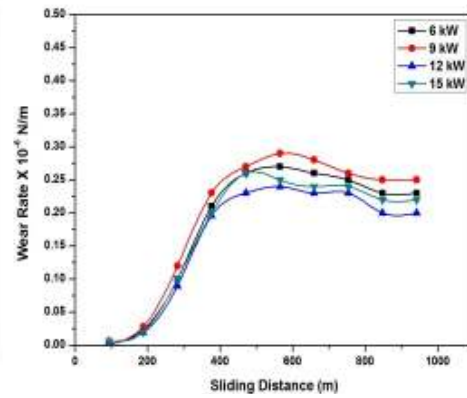


(b)



288

(c)



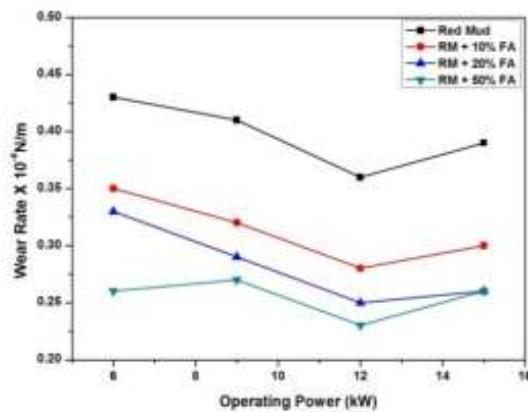
(d)

289

Figure 6. Wear rate comparison for different operating power level. (a) Red Mud, (b) Red Mud +10 % Fly Ash, (c) Red Mud+20% Fly Ash, (d) Red Mud+50% Fly Ash.

290

291



292

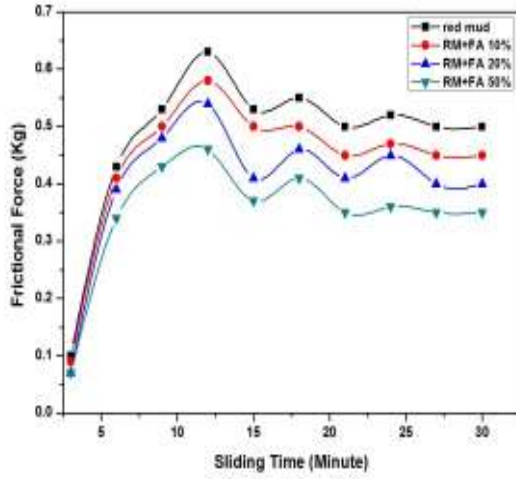
293

294

Figure 7. Variation of wear rate with operating power level at sliding time of 15 minute.

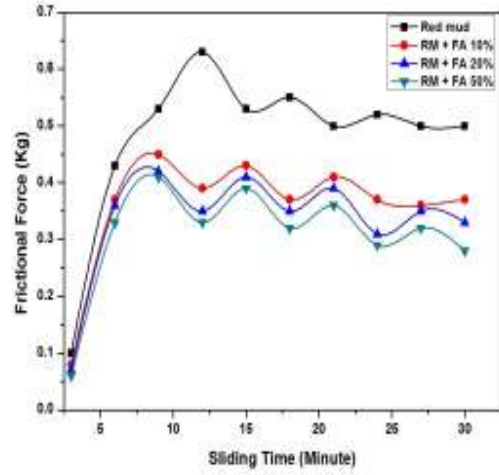
295

296



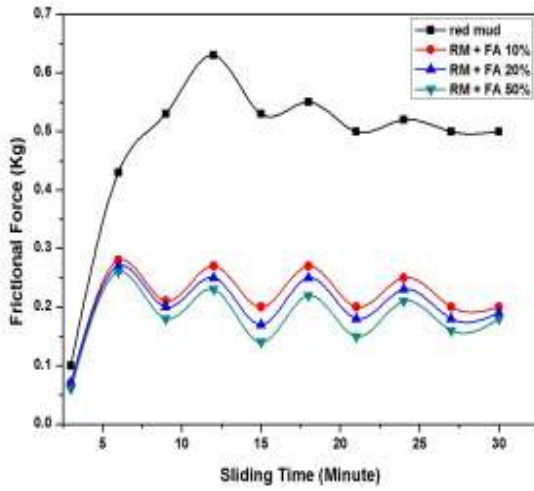
297

(a)



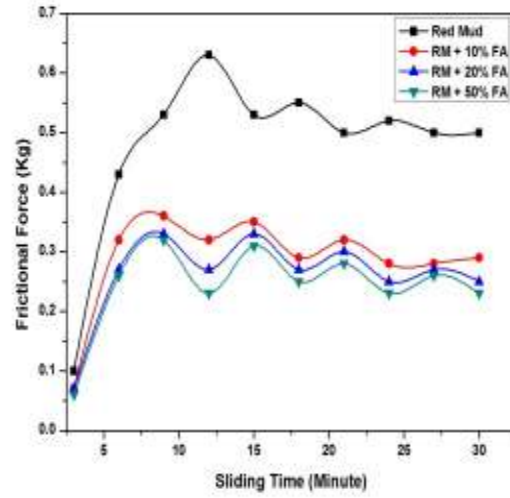
(b)

298



299

(c)

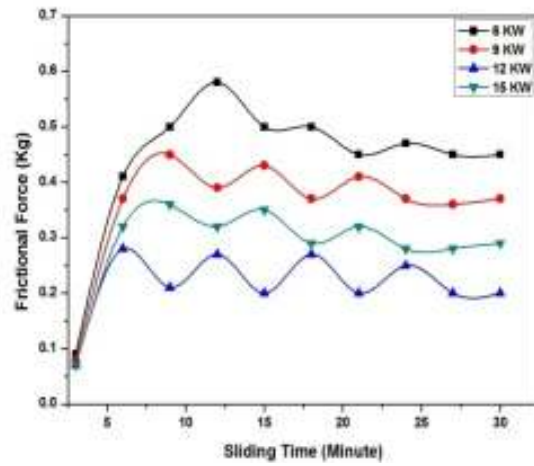


(d)

300

301

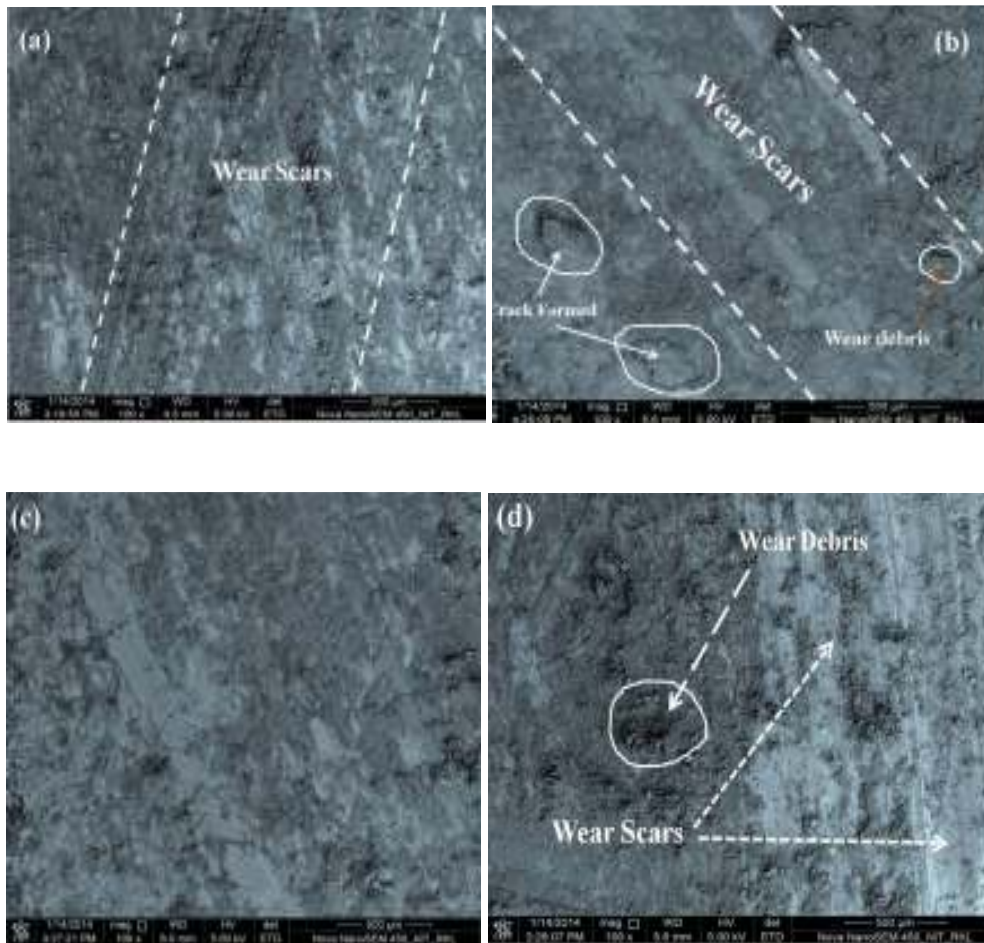
302 Figure.8. Frictional forces against sliding time for all coating type. (a) 6 kW, (b) 9 kW, (c) 12  
303 kW, (d) 15 kW.



304

305

Figure.9. Comparison of frictional force values for 10 % fly ash coating.



306

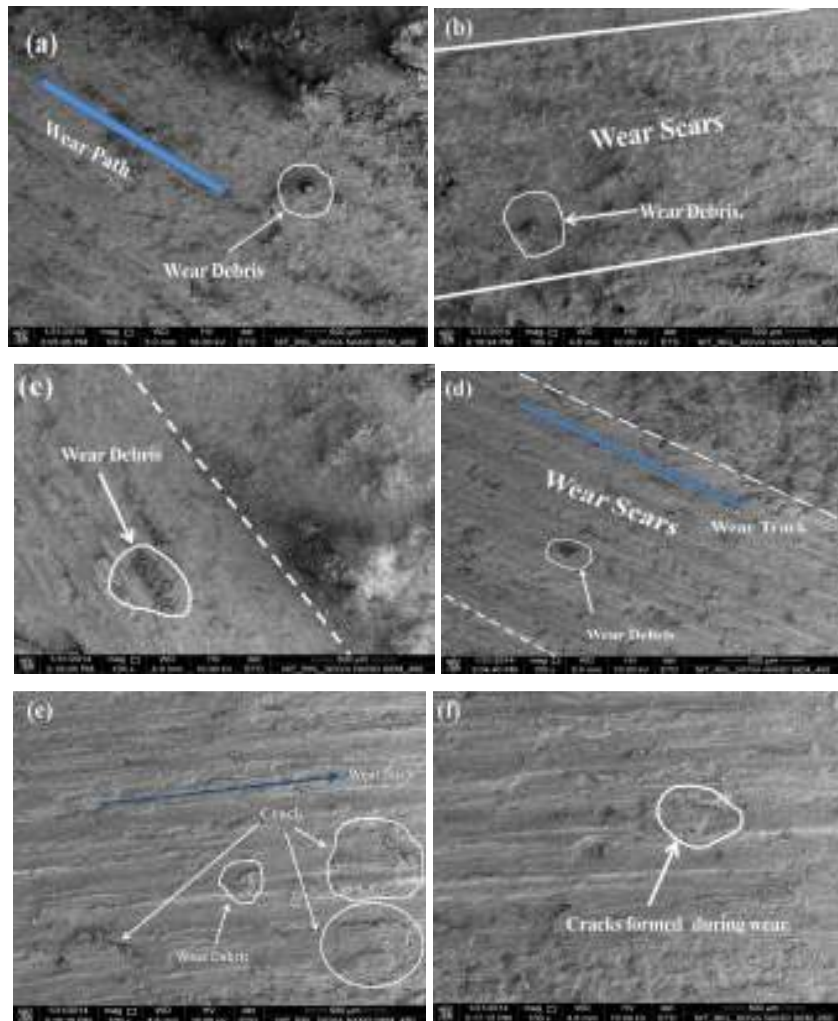
307

308

309

310

Figure.10. Worn Surfaces for Red Mud + 10 % Fly ash coatings for 6kW Operating Power Level.; (a) 3, (b) 6, (c) 12 and (d) 15 minutes time interval.



311

312

313

314 **Figure.11. Worn Surfaces for Red Mud + 50 % Fly ash coatings for 12 kW Operating**  
 315 **Power Level.; (a) 3, (b) 6, (c) 12 ,(d)15, (e) 27 and (f) 30 minutes time intervals.**

316

317 **4. CONCLUSION**

318 The present experimental investigations are being winded up with some salient concluding  
 319 remarks. Red mud, the waste generated from alumina plants is eminently coat able on metal  
 320 substrates by employing thermal plasma spraying technique with excellent wear resistance.  
 321 The addition of fly ash with red mud reduces the wear rate by enhancing the coating property.  
 322 But the optimum percentages of fly ash required for better coating material still impact a  
 323 question mark for the researchers. It is observed that for the early stage the wear rate increases  
 324 slowly and then drastically improved with sliding distance for all coating type and finally  
 325 becomes stagnant. Operating power level proved to be the remarkable variable for coating  
 326 property; which enhances the coating resistance, but afterwards with reaching an optimum  
 327 value indicating some other dominating parameters. The present work leaves with some wide  
 328 spectrum of scopes for future investigators to explore many other aspects of red mud coatings.

329 Thermal stability of these coatings may be evaluated for better claiming in high temperature  
330 applications. Corrosive wear behavior under different operating conditions may be  
331 investigated to identify suitable application areas. Post heat treatment of these coatings may  
332 also be implemented further for furthering the study regarding the improvement in coating  
333 quality and properties.  
334

### 335 **CONFLICT OF INTEREST**

336 The authors declare no conflict of interest exist for publishing this paper.

### 337 **References**

- 338 1. Kushner, B.A and Novinski, E.R. "Thermal spray coating," *ASM Hand book*, **18** (829-  
339 833).1992.
- 340 2. Crook, P; "Friction and wear of Hard facing Alloy," *ASM Hand book*, **18** (758-765),  
341 1992.
- 342 3. Mishra,S.C., Das, S.,Satapathy, Alok., Ananthapadmanabhan P.V., and Sreekumar,  
343 K.P, "Erosion Wear Analysis of Plasma Sprayed Ceramic Coating Using the Taguchi  
344 Technique," *Tribology Transactions*, 2009, vol.52, no.3, pp. 401-404.
- 345 4. Ay, N., Nuri Çelik,O., and Göncü, Y, "Wear Characteristics of Traditional Manganese  
346 Phosphate and Composite hBN Coatings," *Tribology Transactions*, 2013, vol.56, no.6,  
347 pp 1109-1118.
- 348 5. Afzal, M., Ajmal, M., and Khan, A. N, "Wear Behavior of WC-12% Co Coatings  
349 Produced by Air Plasma Spraying at Different Standoff Distances," *Tribology  
350 Transactions*, 2014, vol.57,no.1, pp 94-103.
- 351 6. Wayne,S.F., Sampath., S and Anand, V, "Wear Mechanisms in Thermally Sprayed  
352 Mo-Based Coatings", *Tribology Transactions*, 1994, vol.**37**, no.3, pp :636-640.
- 353 7. Wang, Y., Jin,Y and Wen,S, "The analysis of the friction and wear mechanisms of  
354 plasma-sprayed coatings at 450°C," *Wear*, 1998, vol.**128** , pp. 265–276.
- 355 8. Wang, Y., Jin,Y and Wen,S, "The analysis of the chemical structure and properties of  
356 ceramic surface films in friction using SEM, AES and Micro-region X-ray  
357 diffraction," *Wear*, 1998, vol.**128**, pp. 277–290.
- 358 9. Wang, Y., Jin,Y and Wen,S, "The inspection of sliding surface and subsurface of  
359 plasma-sprayed using scanning acoustic microscopy," *Wear*, 1998, vol.**134**, pp. 399–  
360 411.
- 361 10. Vijande-Diaz,R., Belzunce,J., Fernandez,E., Rincon, A and Pérez,M.C ,Wear and  
362 microstructure in fine ceramic coatings, *Wear*, 1991,vol.**148**, pp. 233–331.
- 363 11. Wei,J and Xue,Q, "Effects of additives on friction and wear behaviour of Cr<sub>2</sub>O<sub>3</sub>  
364 coatings," *Wear*, 1993, vol.**160** , pp. 61–65.
- 365 12. Homberg, K., Mathews,A and Ronkainen, H, "Coatings Tribology-Contact  
366 mechanisms and surface design," *Tribology International*,1998, **31**(1-3), pp 107-120.

- 367 13. Sutar,H., Mishra,S.C., Sahoo,S.K., Chakraverty,A.P. and Maharana,H.S,“Progress of  
368 Red Mud Utilization: An Overview,” *American Chemical Science Journal*, 2014 ,  
369 vol.4,no.3, pp 255-279.
- 370 14. Sutar, H., Mishra, S.C., Sahoo, S.K., Satapathy, A and Kumar, V., “Morphology and  
371 solid particle erosion wear behaviour of red mud composite coatings.” *Natural*  
372 *Science*, 2012,vol.4, no.11, 832-838.
- 373 15. Satapathy,A., Sutar,H., Mishra,S.C and Sahoo,S.K, “Characterization of Plasma  
374 Sprayed Pure Red Mud Coatings: An Analysis,” *American Chemical Science*  
375 *Journal*,2013, vol.3 no.2, pp 151-163.
- 376 16. Prasad,N., Sutar,H., Mishra,S.C., Sahoo,S.K and Acharya,S.K, “Dry sliding wear  
377 behavior of aluminium matrix composite using red mud an industrial waste,”  
378 *International Research Journal of Pure and Applied Chemistry*,2013, vol.3,no.1, pp  
379 59-74.
- 380 17. Pawlowski, L,“The Science and Engineering of Thermal Spray Coatings,” John Wiley  
381 and Sons, New York , pp. 218, 1995.
- 382 18. Satapathy, A., “Thermal Spray Coating of Red mud on Metals” *PhD Thesis*, National  
383 Institute of Technology, Rourkela, Odisha, India, 2005.  
384
- 385